From Force Fields to Dynamics: Classical and Quantal Paths

Donald G. Truhlar; Mark S. Gordon

Science, New Series, Vol. 249, No. 4968 (Aug. 3, 1990), 491-498.

Stable URL:
http://links.jstor.org/sici?sici=0036-8075%2819900803%293%3A249%3A4968%3C491%3AFFFTDC%3E2.0.CO%3B2-W

Science is currently published by American Association for the Advancement of Science.

From Force Fields to Dynamics: Classical and Quantal Paths

DONALD G. TRUHLAR AND MARK S. GORDON

Reaction path methods provide a powerful tool for bridging the gap between electronic structure and chemical dynamics. Classical mechanical reaction paths may usually be understood in terms of the force field in the vicinity of a minimum energy path (MEP). When there is a significant component of hydrogenic motion along the MEP and a barrier much higher than the average energy of reactants, quantal tunneling paths must be considered, and these tend to be located on the corner-cutting side of the MEP. As the curvature of the MEP in mass-scaled coordinates is increased, the quantal reaction paths may deviate considerably from the classical ones, and the force field must be mapped out over a wider region, called the reaction swath. The required force fields may be represented by global or semiglobal analytic functions, or the dynamics may be computed "directly" from the electronic structure results without the intermediacy of potential energy functions. Applications to atom and diatom reactions in the gas phase and at gas-solid interfaces and to reactions of polyatomic molecules in the gas phase, in clusters, and in aqueous solution are discussed as examples.

THE DEVELOPMENT OF PRACTICAL AND ACCURATE METHODS to treat the dynamics of chemical reactions is a critical challenge to theoretical chemistry. Most approaches involve two steps—the standard approach is first to use some means to determine or approximate as much as possible of the potential energy function (PEF) (*1*) and then to use that PEF as a starting point for investigations of the dynamics. In principle, it is desirable to know the dependence of the PEF on a wide range of all variables, but this becomes increasingly impractical as the complexity of the reaction increases, so computational efforts must be focused on essential features.

Many approaches have been used for mapping PEFs for chemical reactions. One method is to fit an analytic PEF so that dynamics calculations agree with available experimental rate data. The diatomics-in-molecules procedures developed from the early work of London, Eyring, Polyanyi, and Sato (*2*) (often referred to as the LEPS or generalized LEPS method) have been very useful for such semiempirical functions. This approach has been used for many years, for example, for the H + H_2 and Cl + H_2 reactions (*3*).

D. G. Truhlar is in the Department of Chemistry and the Supercomputer Institute, University of Minnesota, Minneapolis, MN 55455. M. S. Gordon is in the Department of Chemistry, North Dakota State University, Fargo, ND 58105.

In recent years the capability to perform accurate electronic structure calculations of PEFs has improved dramatically (*4, 5*), and it is now possible to improve upon the purely semiempirical approach by fitting ab initio or semiempirical electronic structure calculations at important points on the PEF or by combining electronic structure calculations for certain features of the PEF with additional refinement based on comparing dynamics calculations to experiment. For reactions with more than four atoms, for example, the reaction of CH_3 with H_2 (*6, 7*), the LEPS approach is sometimes applied to atoms involved in bond breaking and making and combined with "molecular mechanics"–type models for nonbonded interactions. Other approaches are reviewed elsewhere (*8*). Determination of the critical geometries, interpolation of the electronic structure results, and analytic representation of the whole PEF from information at selected points is a stimulating challenge to the dynamicist's skill and experience, and it allows for the artful interplay of theory and experiment. Nonetheless, it is often preferable for such investigations to be more systematic in order to allow a wider range of applications.

In order to capture most of the physics while keeping our treatment computationally tractable, we need to ignore large parts of the PEF. The first step in such a development is the recognition of key topological features of PEFs that must be treated as accurately as possible for reactive systems. The most significant of these are the points that have a zero gradient of the energy with respect to atomic coordinates and therefore correspond to stationary points. If the matrix of second derivatives of the potential energy with respect to atomic coordinates (hessian) at such a point is positive semidefinite, then the point is a local minimum. If the hessian has one (and only one) negative eigenvalue, then the associated eigenvector gives the direction of (downhill) motion to reactants and products, and the point is a saddle point. In conventional transition state theory (TST) (*9*), rate constants for chemical reactions are approximated entirely on the basis of the geometries, energies, and energy derivatives at stationary points (by the calculation of the appropriate partition functions from molecular structures and vibrational frequencies). This approach provides a simple model for the prediction of Boltzmann-averaged rate coefficients. Modern techniques in electronic structure theory now make it relatively straightforward to determine the gradient and hessian at enough geometries to find and characterize the stationary points even for many-atom systems (*10*).

In many cases we are not satisfied with a description based only on stationary points or with only calculating thermal rate coefficients, and we seek to map out and utilize a larger portion of the interaction space, including the minimum-energy valleys connecting reactants and products to saddle points and the ridges through which reactions may proceed by tunneling. These features certainly affect rate constants significantly in many cases, and in addition they

are crucial for determining state-to-state cross sections, especially when the product energy distribution is nonstatistical. We find that generalized transition state theory and semiclassical tunneling methods allow us to base calculations of rate constants, threshold energies, and tunneling probabilities on the most critical parts of the PEF without having a global representation of this function. The most systematic way to calculate these critical PEF features is to begin with the steepest descents paths that connect saddle points to minima. Such a path is referred to as a minimum energy path (MEP). Physically intuitive approximations to the dynamics in the vicinity of an MEP [such as one-dimensional (1-D) tunneling, internal centrifugal effects, vibrational adiabaticity, and infinitely damped trajectories] are facilitated when the path is calculated in isoinertial coordinates, that is, in any coordinate system that is mass scaled to make the effective reduced mass the same for all atomic displacements [a familiar example is the mass-weighted system (*11*) of infrared spectroscopy in which the effective reduced mass is chosen as 1 amu]. The MEP in an isoinertial coordinate system (*12–16*) is sometimes referred to as the intrinsic reaction coordinate (IRC) (*15*), and we use the two terminologies (MEP and IRC) as synonyms.

When potential energy contours are plotted in isoinertial coordinates, the angle (commonly called the skew angle) between the reactant and product valleys depends on the mass combination, and hence so does the curvature of the MEP. This is illustrated in Fig. 1, which shows four examples of MEPs: that for the H + D_2 reaction has small curvature because the skew angle is 65.9°; those for O + H_2 and Cl + HD have medium curvature and skew angles of 46.7° and 36.4°, respectively; and that for Cl + HCl′ (where Cl denotes ^{35}Cl and Cl′ denotes ^{37}Cl) has large curvature because the skew angle is only 13.4°. The physical meaning of the skew angle follows from the fact that mass scaling converts mass effects into relative distances. Thus, for example, in a light-atom transfer, the motion from the reactant valley to the product valley corresponds to a small reduced mass and hence a fast motion—thus in mass-scaled coordinates the two valleys must be very close, resulting in a small skew angle.

Knowledge of the sequence of geometries along the MEP allows one to calculate the curvature of the path and hence the reaction path kinetic energy (*13, 17–20*), and knowledge of the potential along the path and the force constants for motion transverse to it allows one to write a convenient reaction-valley potential (*13, 14, 17, 18, 21*) for low-energy dynamical motions connecting reactants and products. One method based on such information is variational transition state theory (VTST). VTST uses a criterion of minimum flux (*22*), maximum vibrationally adiabatic energy (*23, 24*), or minimum free energy of activation (*20, 21, 24–26*) to determine a dynamical bottleneck for overbarrier processes, which tend to involve only motions in the vicinity of the MEP. When the curvature of the MEP is small, realistic tunneling probabilities can also be calculated entirely from the reaction path, its curvature, and the reaction-valley potential (*20, 27, 28*). When, however, the MEP is highly curved, tunneling may proceed by shortcuts through regions beyond the radius of curvature of the MEP (*29, 30*) as illustrated in Fig. 1C; such regions are wider than the valley that can be described in curvilinear coordinates based on the path itself. Then the reaction path, its curvature, and the reaction-valley potential do not provide enough information for an adequate treatment of reaction dynamics, and one needs to explore a region adjacent to the reaction path called the reaction swath. In either the small- or large-curvature cases, the effects of tunneling may be incorporated into VTST by a ground-state transmission coefficient (*20, 28, 30, 31*).

In the present article, we discuss the use of minimum energy paths, reaction-valley potentials, and quantal tunneling paths for reaction dynamics. First we discuss the essential features of variational transition state theory and semiclassical treatments of tunneling. This is followed by a discussion of reaction paths, reaction-path force fields, dynamics, and recent applications.

Variational Transition State Theory

A generalized transition state (GTS) is a hypersurface in phase space (which is the space of all position and momentum coordi-

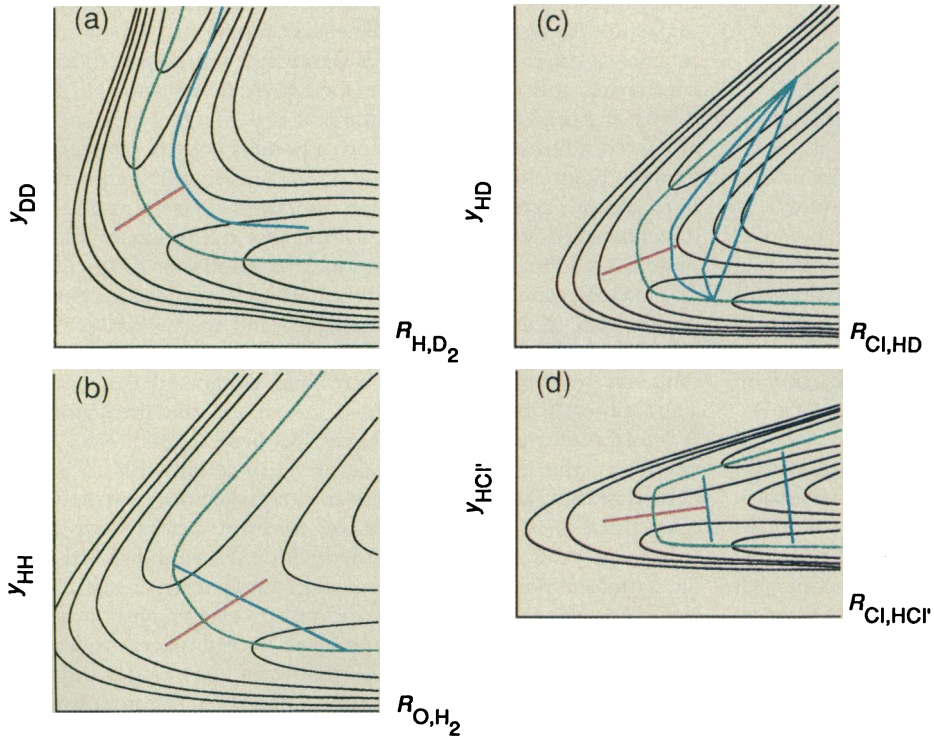

Fig. 1. Potential energy contours (black), transition states (red), minimum energy paths (green), and tunneling paths (blue) for four representative reactions A + BC → AB + C in isoinertial coordinates. $R_{A,BC}$ is the distance from A to BC; γ_{BC} is the mass-scaled distance between B and C; and only collinear geometries are illustrated. The transition states are surfaces dividing reactants from products; they are located at the saddle point and have zero-point vibrational amplitude for the vibration transverse to the minimum energy path. The reaction proceeds from lower right to the top of the figure in each case. (**A**) H + D_2 → HD + D. The tunneling path is a Marcus-Coltrin path (*24, 27*), which is appropriate for small-curvature systems. (**B**) O + H_2 → OH + H. The tunneling path is the optimum LAG path (*39, 69*) for a typical tunneling energy at room temperature. (**C**) Cl + HD → HCl + D. The tunneling paths are three trial paths for a least-action tunneling calculation (*39*) at a typical tunneling energy. The optimum tunneling path in this case is between the two blue curves lying closest to the green curve. (**D**) ^{35}Cl + H^{37}Cl → H^{35}Cl + ^{37}Cl. The tunneling paths are large-curvature paths (*30*) for two different energies: the one farther from the green curve for a typical tunneling energy and the one closer to the green curve for a higher energy.

nates) or coordinate space that divides reactants from products (*21, 22, 31*). The conventional transition state is a special case depending only on coordinates (not momenta) and passing through the saddle point; it is constrained to be a hyperplane in isoinertial coordinates and to be perpendicular to the imaginary frequency normal mode. It can be shown (*22*) that in classical mechanics under thermal equilibrium conditions of the reactant [which conditions are usually assumed to hold (*32*)] the rate coefficient $k(T)$ is bounded from above by the one-way flux coefficient $k^{GT}(T)$ for passage through any GTS, and if the GTS is varied without constraints, then min $k^{GT}(T) = k(T)$. This is the basis for VTST: we vary the GTS to minimize the calculated flux coefficient, and the minimum value is accepted as an approximation to $k(T)$. The GTS corresponding to the minimum flux constitutes a "dynamical bottleneck" to the reaction.

The theory as presented above is not useful for two reasons: (i) for an N-atom system, phase space has $6N$ dimensions, and unconstrained variations of the GTS are impractical; and (ii) quantum effects, especially zero-point motions and tunneling, are very important, and classical mechanics is inadequate. Current practical VTST and tunneling methods (*20, 24, 26, 31, 33*) have evolved as a way to overcome these limitations.

The signed distance along the MEP from the saddle point, measured in the isoinertial coordinate system, is called s. We define a one-parameter sequence of GTSs, where the parameter is the value of s at which the GTS crosses the MEP. Each GTS is, at least in the vicinity of the MEP, a hyperplane in isoinertial coordinates and orthogonal to the MEP at the point of intersection.

Practical VTST calculations are carried out as follows: First the MEP is calculated on a grid with stepsize δs; this requires at least one gradient evaluation for each step. Then, at typically larger intervals Δs, one calculates the curvature components and a hessian and perhaps higher derivatives depending on whether anharmonicity (*33, 34*) is to be included in the partition functions. At these hessian points one also calculates the GTS standard-state molar-free energy of activation $\Delta G^{GT,0}(T,s)$ for each temperature of interest. The curve of $\Delta G^{GT,0}(T,s)$ as a function of s is called a free energy of activation profile. The VTST rate constant for a canonical ensemble at temperature T is given by (*21, 24, 26*)

$$k^{CVT}(T) = \min_s (k_B T/h) K^0 \exp[-\Delta G^{GT,0}(T,s)/RT] \quad (1)$$

where CVT denotes canonical variational theory, k_B is Boltzmann's constant, h is Planck's constant, K^0 is the reciprocal of the standard state concentration for bimolecular reactions and is unity for unimolecular reactions, and R is the gas constant. Thus the variational transition states are the maxima with respect to s of $\Delta G^{GT,0}(T,s)$.

At low temperature, the variational transition state, which is the location of the minimum in Eq. 1, occurs at the maximum of the vibrationally adiabatic(a) ground-state(G) potential curve defined by (*20, 26*)

$$V_a^G(s) = V_{MEP}(s) + \varepsilon_{int}^G(s) \quad (2)$$

where $V_{MEP}(s)$ is the Born-Oppenheimer potential along the MEP, and $\varepsilon_{int}^G(s)$ is the local zero-point energy. Thresholds for vibrationally excited reactants or products are well approximated by the maxima of excited-state analogs of Eq. 2 when the excited vibrations are high-frequency modes and there are no avoided crossings or regions of high reaction-path curvature between the maximum and the corresponding reactant or product (*35, 36*). Such effective potential curves, corresponding to conservation of vibrational quantum numbers orthogonal to the MEP, are called "vibrationally adiabatic."

The functions $\Delta G^{GT,0}(T,s)$, $V_a^G(s)$, and $V_{MEP}(s)$ that appear in Eqs. 1 and 2 are illustrated in Fig. 2 for the isomerization of planar :Si=SiH_2 to the nonplanar :Si$\overset{H}{\underset{H}{\equiv}}$Si: in which the hydrogens are attached to the two Si–Si π bonds (*37*). The coordinates are scaled to a mass of 1 amu, and the saddle point, which has the planar structure :Si$\overset{H}{\equiv}$SiH, is taken as the origin of the reaction coordinate, so $V_{MEP}(s)$ peaks by definition at $s = 0$. As the system proceeds along the reactant valley from $s < 0$ to $s = 0$, the dominant vibrational frequency changes are loosenings of the out-of-plane mode and of the Si–H stretching frequency for the first H to migrate. As a result, there is a competition between increasing $V_{MEP}(s)$ and decreasing $\varepsilon_{int}^G(s)$, and $V_a^G(s)$ peaks at $s = -0.15\ a_0$, which is therefore the location of the variational transition state (VTS) at 0 K. At finite temperatures, vibrational entropic effects reinforce the shift of the VTS from the saddle point, and Fig. 2 shows that it moves progressively farther toward reactants as T increases (*37*). Thus it is necessary to consider system properties at locations removed from the saddle point to find the dynamical bottleneck.

Tunneling

The most practical accurate methods to calculate tunneling probabilities are semiclassical. The semiclassical approach to tunneling (*38*) is to find a dominant tunneling path or set of tunneling paths and calculate the exponential decay of the wave function along such paths in terms of a 1-D path integral involving the multidimensional action along the path. The tunneling probability is basically the square of the wave function on the other side of the barrier, although in practice a uniformized expression is used. In general the best tunneling paths are the ones that minimize the exponential decay of the wave function, that is, most of the tunneling flux is carried by the highest-probability paths. This involves a compromise between tunneling where the barrier is lowest (along the MEP) and where the tunneling path is shortest (through the potential ridge on the concave side of the MEP as shown in Fig. 1).

In the limit of large reaction-path curvature, the optimum tunneling paths are determined entirely by the length factor in isoinertial coordinates and so they are straight lines from the reactant valley to the product one (*30, 31*). In the general case, however, the best tunneling path is determined numerically from among a sequence of trial paths (*31, 39*). In the limit of small reaction-path curvature, a simple limiting approximation becomes valid, and the exponential decay can be estimated by using only $V_a^G(s)$, the reaction-path curvature components, and the distances $t_v(s)$ of the various modes v to the concave-side turning points as function of s (*27, 28*).

The limiting-case tunneling methods for VTST-plus-tunneling (VTST/T) calculations for small and large reaction path curvature are called the small-curvature semiclassical adiabatic ground-state (SCSAG) (*28*) and large-curvature ground-state, version 3 (LCG3) (*31, 39, 40*) approximations, respectively. The method based on numerically searching for the least-imaginary-action tunneling path is called the least-action ground-state (LAG) (*31, 39*) approximation.

The thermally averaged tunneling probability yields a transmission coefficient $\kappa(T)$, which is multiplied by $k^{CVT}(T)$ to yield the final estimated rate coefficient.

Global Energy Functions

Global energy functions are analytic representations defined for and as accurate as possible for all values of all coordinates. A wide

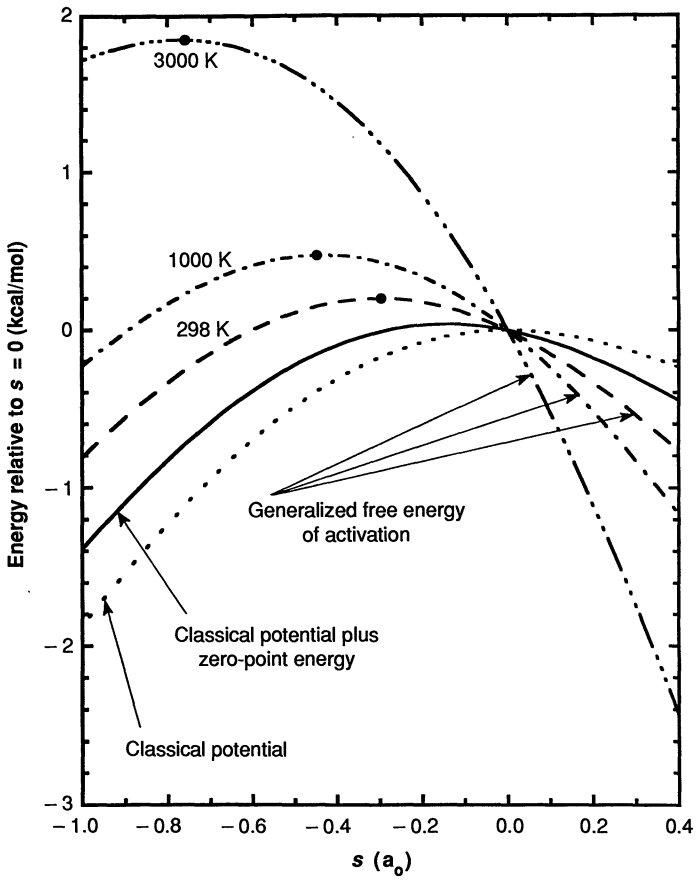

Fig. 2. $V_{MEP}(s)$, $V_a^G(s)$, and $\Delta G^{GT,0}(T,s)$ for T = 298, 1000, and 3000 K as functions of reaction coordinate s (*37*). The zero energy for each curve is located at the conventional transition state (s = 0). The locations of the three finite-temperature variational transition states are indicated by heavy dots.

variety of methods have been used to obtain approximate global PEFs for simple reactions. The most straightforward approach is to perform a large number of electronic structure calculations and fit the results with the use of least squares. Examples of reactions for which this procedure has been followed include H + H_2 (*41*); O + H_2 (*8, 42*), Cl + HCl′ (*8, 30*), He + H_2^+ (*43*), HeH^+ + H_2 (*44*), OH + H_2 (*45*), and others (*8*). Ab initio data has also been used as a guide to model the PEF, for example, for the unimolecular dissociations of methane (*46*), silane (*47*), and ethyl radical (*48*), and for the reaction CH_3 + H_2 → CH_4 + H (*7*). Ideally, an initial fit to the ab initio data is used for preliminary tests of the sensitivity of the dynamics to surface features, and these tests are used to guide the computation of additional points on the PEF.

A limitation to the construction of a global PEF with the aid of ab initio calculations is the computational expense of performing a large number of such calculations with sufficient accuracy, especially as the size of the system of interest increases. One alternative is to use an empirical or semiempirical functional, with little or no input from electronic structure calculations. For example, the diatomics-in-molecules method, discussed at the beginning of this article, may be used to approximately express the potential of a polyatomic species in terms of information about its atomic and diatomic fragments. It is sometimes necessary to add additional terms (*49*) to obtain realistic PEFs, and the diatomics-in-molecules approach can also be made more flexible by making the parameters in the corresponding equations be functions of key structural variables (such as bond lengths and bond angles) (*50, 51*). The diatomics-in-molecules approach has been used to model systems such as H_3^+ (*52*), SiH_2 (*53*), and CH_n (n = 2 to 4) (*54*). It is encouraging that some of the techniques developed originally for three-body systems can be used profitably for portions of semiglobal surfaces for larger systems (*7*), but it is also important to emphasize that diatomics-in-molecules techniques are very sensitive to the available input data (*55*). A very appealing approach is to determine some parameters in the PEF based on electronic structure calculations (for example, of saddle point frequencies) and to adjust other parameters (for example, those which determine the barrier height) on the basis of trial-and-error, such as by comparing predictions of VTST/T calculations to experimental thermal rate constants or the predictions of other dynamical methods to more detailed experimental data. [An example of the latter is the use of state-specific vibrationally adiabatic barrier heights based on exit-channel reaction paths to predict experimental product-state–specific reaction thresholds for the F + H_2 reaction (*51*).] This kind of combined ab initio–semiempirical treatment can provide useful approximations to full or semiglobal PEFs as required for full quantum dynamics calculations, but—as discussed in the introduction—it involves considerable "art" as well as science, and each new PEF is a major undertaking. This difficulty motivates the reaction-path approach.

Very recently it has been shown (*56*) that semiempirical molecular orbital theory parameterized for individual reactions may be used successfully in lieu of an analytic PEF for semiclassical rate calculations, and it will be interesting to carry out further calculations to learn the sensitivity of the results to the individual parameters. Another approach, discussed next, allows such dynamics calculations to be based on more reliable ab initio electronic structure calculations.

Reaction-Valley Potentials

If one is to generate a reaction-valley potential directly from ab initio electronic structure theory, a major concern is the efficiency of methods for following the MEP. Considerable effort has been expended to develop accurate algorithms for this purpose (*57–65*). The specific concern here is to allow as large a step along the MEP as possible (to minimize the number of time-consuming evaluations of the function and its gradient) while keeping the deviations of the computed path from the true MEP small.

Several candidates can be considered in choosing a method for determining the MEP for direct dynamics calculations (*57–65*). The simplest of these is to use only a gradient evaluation at the previous step to generate the MEP; this is the Euler single-step (ES) algorithm. In the Euler-stabilization methods (*57, 60, 62*), a correction is applied that often allows the step size to be increased by a factor of 3 to 5, so although more function evaluations are required per step, there is a net gain in efficiency. For flat surfaces, the fourth-order Runge-Kutta method (*60*) may lead to a converged MEP with a larger step size than the ES and Euler stabilization methods, but it requires much more work per step. For stiff systems, in which the changes in geometric variables along the path are quite different from each other, it is still not clear which algorithm is best.

As a general step, the methods above require only evaluations of the energy or gradient or both. They are initiated, to lowest order, by generating the hessian at the saddle point, diagonalizing it to get normal modes, and making a small step off the saddle point in the direction indicated by the normal coordinate associated with the imaginary frequency. Page and McIver (*59*) have developed a method to generate the MEP that uses a cubic derivative at the saddle point and makes use of second derivatives elsewhere. In some cases, although the step size this allows is greater than for energy-and-gradient methods, it requires a sufficiently larger number of second derivatives that it is more time-consuming than the energy-

and-gradient methods (*65*). An improved version (*63*) of this algorithm may allow even larger steps, however, and could become the method of choice.

The degree to which an MEP has been adequately converged is difficult to quantify, but the convergence is best related to the properties that are needed in order to obtain the reaction-valley potential or to calculate a rate constant. In order of increasing sensitivity, these are the electronic energy, molecular structural parameters, vibrational frequencies, vibrational coupling coefficients [$B_{k,k}$ (*19, 58*)], and reaction path curvature. The molecular structure and projected vibrational frequencies along the path are needed for the evaluation of rotational and vibrational partition functions by GTS theory. In addition, these quantities themselves provide a useful "picture" of the course of the reaction. The vibrational frequencies also permit the evaluation of the zero-point vibrational energy corrections to the electronic energy along the path, as required for the vibrationally adiabatic potential curve. Combined with the structures, one can then calculate the entropy corrections and therefore the free energy of activation profile at any temperature. This is the central quantity of canonical VTST. To evaluate a quantitative rate constant, it is often necessary to include tunneling and to obtain the reaction path curvature. The curvature components are difficult to converge and provide the most sensitive test of the various methods for obtaining an MEP.

Reaction Swaths

When tunneling in regions far from the MEP is important, the next step is to study the reaction "swath," in which additional regions of configuration space on the concave side of the reaction valley or tube are probed. Only limited information about the reaction swath is obtained from any potential expanded in reaction-path coordinates, even by using the anharmonic potentials along the generalized normal modes. It is also necessary to calculate selected points beyond the radii of curvature for all modes with large curvature components.

For highly curved reaction paths, as occur for example when a light atom such as hydrogen is being transferred between two heavy atoms, the likelihood of "corner cutting" by tunneling is greatly increased (*29, 30, 66*). Then one must calculate additional ab initio points in the tunneling region in order to obtain a more realistic PEF.

Atom-Diatom Reactions

For several atom-diatom reactions with small-to-intermediate reaction path curvature it has been possible to compare rate constants calculated by the VTST/SCSAG method to the results of accurate quantum dynamics for the same PEF. These reactions include H + H_2 → H_2 + H, O + H_2 → OH + H, and H + H′Br → Hbr + H′, as well as two isotopically substituted analogs of the first reaction and three of the second (*67*). For all eight cases at 300 K, the average deviation of VTST calculations with small-curvature transmission coefficients from accurate quantum dynamics is 37%, and the average deviation of the VTST calculations with least-action transmission coefficients results from the accurate ones is only 13%! This is very encouraging for the reliability of tunneling calculations based on the MEP and reaction-valley potentials and of those based on the more general least-action paths; it gives added confidence for cases where these methods are applied in more complicated systems where comparison to accurate dynamics is not feasible.

Typical intermediate-curvature systems for which least-action optimizations of tunneling paths are important are Cl + HD → HCl + D or DCl + H, O + H_2 → OH + H, and O + HD → OH + D or OD + H. Three of the trial tunneling paths in the one-parameter sequence used for a LAG calculation on the first of these reactions are shown in Fig. 1C. In this case, the semiclassical tunneling calculations were tested against accurate quantum mechanical calculations for the collinear reaction (*39*). Whereas the accurate quantum rate constants require a transmission coefficient of 8 at 200 K, tunneling along the MEP yields only 2. Optimizing the tunneling path by the LAG method yields 6, in much better agreement with full quantum dynamics. LAG calculations of cumulative reaction probabilities have recently been compared to accurate quantal ones for full 3-D reaction probabilities as small as 10^{-7} or smaller in the O reaction cases, and the agreement is very good (*68, 69*). For the O + H_2 reaction, tunneling along the MEP yields a transmission coefficient of 4 at 297 K, whereas the LAG method, based on appreciable corner cutting, yields 13 and gives excellent agreement with experiment; the optimum semiclassical tunneling path (*69*) for a typical tunneling energy at room temperature is shown in Fig. 1B.

An example of a reaction with large reaction-path curvature is ^{35}Cl + $H^{37}Cl$ → $H^{35}Cl$ + ^{37}Cl. This reaction has been studied with a partly ab initio, partly empirical PEF obtained as discussed above (*30*). Even though the ab initio saddle point on this PEF is symmetric and has H–Cl distances R_1 and R_2 of 1.47 Å, the variational transition state has R_1 = 1.60 Å and R_2 = 1.35 Å, with the latter value being much closer to the diatomic HCl value of 1.27 Å. Both transition state locations have $R_1 + R_2$ = 2.94 to 2.95 Å, but the thermal rate constant at room temperature is dominated by tunneling in configurations with $R_1 + R_2 \geq 3.2$ Å. An example of such a path is shown as the right-most blue tunneling path in Fig. 1D. Comparisons to accurate quantal dynamics show good agreement for total reaction probabilities in collinear collisions (*30*) and reaction rate constants in 3-D (*70*). The 3-D reaction cross sections are dominated by high rotational states, which correlate to high-bend excited states at the transition state. Thus the success of the ground-state tunneling models results at least in part from rotational nonadiabaticity, which allows the phase-space flux from excited reactants to pass through the critical configurations for tunneling in the ground vibrational state. Further study of such effects would be very interesting. Vibrationally nonadiabatic tunneling has also been studied (*66, 71*).

Large-curvature tunneling calculations on three-body systems have also been used as models for more complicated systems such as hydride transfer between nitrogen heterocycles (*71*). Phenomenological analysis of isotope effects on Brønsted plots for such reactions, guided by these model studies, indicate that tunneling occurs in more extended nuclear frameworks [larger C–C distances in $\widehat{RCH}^+ + \widehat{R'CH_2} \rightarrow \widehat{RCH_2} + \widehat{R'CH}^+$, where R and R′ denote the remainders of the heterocyles and $\widehat{RCH}^+$ is an NAD^+ (nicotinamide adenine dinucleotide) analog] for protide transfer than for deuteride transfer. Nuclear tunneling between the two equivalent isomers of malonaldehyde provides an example of a large-curvature tunneling system that has been studied in more dimensions, albeit with different methods than discussed here (*72*).

Vibrationally adiabatic bottlenecks for reaction of vibrationally excited diatomics have been compared to accurate quantum mechanics for D + H_2 (v = 1) (*73*) and O + H_2(v = 1) (*68*). In both cases the validity of the effective barrier to reaction predicted by the reaction-path calculations (*36*) was verified, although these effective barriers are higher than the ground-state ones and are dramatically far removed from the saddle points.

For calculating tunneling probabilities, the curvature of the MEP is the single most important feature in determining the extent of

corner cutting. Similarly for overbarrier processes, the curvature of the MEP plays a dominant role in controlling the exchange of energy between the reaction coordinate and the reactant and product vibrations (*18, 74*). There is a more detailed analogy between tunneling and overbarrier dynamics for systems with very large curvature. As discussed above, when reaction-path curvature is very large, as in the transfer of a light atom between two heavy moieties, the optimum tunneling path may be so far from the MEP that very little flux from reactant to product actually passes within one ground-state vibrational amplitude of the MEP. Similarly, for overbarrier processes in systems with very large reaction-path curvature, the region around the MEP may be associated with a "white spot" that is not covered by the traces of an ensemble of reactive trajectories (*75*).

Direct Dynamics for Polyatomic Reactions

The prediction of dynamical quantities, including rate constants, directly from ab initio electronic structure theory–minimum energy paths and associated reaction path hamiltonians has been called direct dynamics (*62*). The first applications of direct dynamics involved unimolecular reactions in which approximate MEPs were obtained without discussing convergence with respect to step sizes (*76*). The first application of direct dynamics to a bimolecular reaction was the investigation of the reaction $CH_3 + H_2 \rightarrow CH_4 + H$, in which VTST rate constants including small-curvature tunneling contributions were calculated from ab initio electronic structure input (*62*). The goal was to demonstrate the feasibility of the direct dynamics approach with converged step sizes, so the comparison of the predicted rate constants to experiment was not a primary concern. Nonetheless, the analysis illustrates what we may expect to learn by the direct dynamics approach. For example, the generalized free energy of activation along the MEP shows that the free energy bottleneck moves away from the top of the electronic energy barrier as the temperature increases. The POLYRATE computer program (*7*) was used to calculate the rate constant with tunneling included in the SCSAG approximation. The calculations confirm the conclusion from earlier studies (*37*) with a semiempirical PEF that a realistic treatment of the low-temperature rate process must account for tunneling and the curvature of the reaction path. For example, at 298 K, incorporation of the reaction-path curvature in the tunneling calculation increases the predicted rate by 1.5 orders of magnitude (*62*). This gives more confidence in the earlier calculations (*7*) based on a global PEF, which are in excellent agreement with recent experiments (*78*). An analysis of the generalized normal modes along the MEP in terms of the contributions from each internal coordinate has been very useful in interpreting the reaction path curvature in terms of coupling between the reaction path and the transverse vibrations (*79*).

Another reaction studied both with a global PEF (*33, 35*) and also by direct dynamics (*58*) is $OH + H_2 \rightarrow H_2O + H$. In this case the maxima of excited-state vibrationally adiabatic potential curves (*35, 36*) provide physical and quantitative explanations of the effect of excitation of either diatomic on the reaction rate (*35*), and the terms coupling different vibrational modes orthogonal to the MEP yield qualitative insights into product vibrational-energy distributions (*58*).

Illuminating analyses of the evolution of the electron density as the system proceeds along the MEP have been reported both for $CH_3 + H_2 \rightarrow CH_4 + H$ (*80*) and for $CH_3 + HF \rightarrow CH_4 + F$ (*81*) by Tachibana *et al.* They found strong back donation of electrons from the singly occupied molecular orbital CH_3 to HF in the early part of the latter reaction. Other studies of the evolution of the electronic charge distribution along reaction paths have been presented by Leroy and Fukui and co-workers (*82*).

A rather higher level of theory has been used to study the pseudorotational motion in SiH_5^- (*83*). This is an important process, since (unlike the analogous carbon system) attack of a nucleophilic anion at a silicon center frequently leads to a stable (pentacoordinated) complex that is much lower in energy than the separated reactants. For the prototypical species SiH_5^- the predicted well depth of 16 kcal/mol (*84*) may be compared with the calculated pseudorotational barrier of 2 kcal/mol (*83*) [both calculated at the MP2/6-31++G(d,p) level (*4*) of theory]. These energetics suggest that several pseudorotations may occur before one of the ligands leaves. As the first step in the analysis of this process, the MEP was generated at the MP2/6-31G(d) level with a reduced mass of 1 amu and δs equal to 0.01 a_0 to 0.05 a_0 with the RK4 algorithm. A vibrational analysis (*79*) reveals that there is very little stretch-bend interaction along the MEP and that each stretching motion changes smoothly from a basal or apical stretch at the saddle point to an axial or equatorial stretch at the minimum. Similar comments apply to the bending motions. The next steps in this analysis will be to examine the VTST rate constants and the vibration-to-vibration energy transfer from the S_N2 reaction coordinate into the pseudorotation motion. Similar analysis of the PH_5 pseudorotation (*85*) and the conformational rearrangements of glycine (*86*) is under way.

Houk and Jorgensen and their co-workers (*87, 88*) have applied VTST to the reaction of $:CCl_2$ and other halocarbenes with ethylene in order to gain some insight into the energetics of carbene additions. Although even the most complete calculations (*88*) followed an idealized path, rather than a minimum energy one, they indicate that a π complex between the halocarbene and substrate ethylene is not a generalized transition-state free energy of activation minimum, although it may be an energetic minimum along the MEP. This result suggests that entropy may play an important role in such reactions. Similar effects (*37*) occur in both the $HCN \leftrightarrow HNC$ and $:Si{=}SiH_2$ isomerizations discussed above, where the less stable isomer (HNC or $:Si{=}SiH_2$) becomes a maximum on the GTS free energy of activation curve as the temperature increases. Entropy control is also clearly implicated in association reactions (*89, 90*) and has also been postulated for the isomerization of tetramethylene (*91*) and the abstraction of H from ethyl radical by another H (*92*).

Morokuma and co-workers (*93*) have also presented informative studies of vibrational frequencies and mode couplings along the reaction path for several reactions, and these studies further illustrate how reaction-path analyses lead to interesting physical insights for a wide variety of cases.

Solvation Effects

Reaction-path methods have been used to study solvation effects both in clusters (microsolvation) and in solution (bulk solvation). The first cluster reaction studied by reaction-path methods is (*94*)

$$Cl^-(H_2O)_n + CH_3Cl' \rightarrow ClCH_3 + Cl'^-(H_2O)_n$$

where $n = 1$ or 2. Notice that the water molecules must transfer (*95*) with the charge or the reaction would be quite endothermic. The reaction path was calculated both for the unsolvated primary system (that is, as if n were 0) and also for the full system (with $n = 1$ or 2). In the former case, water was added and allowed to equilibrate to the primary system with its structure fixed at a point on the unsolvated MEP. The variational criterion of VTST was used to select a GTS for each point on the MEP. This calculation corresponds to the organic chemists' concept of equilibrium solvation

(*9*), whereas the "full" calculation allows for nonequilibrium (*96*) solvation. Comparison of the two calculations allowed for a rigorous test of the equilibrium solvation concept. The two sets of results for $n = 1$ agree to 8%, so we conclude that the reaction path in this cluster reaction may be modeled quite adequately with the equilibrium solvation assumption. One can still argue, however, whether nonequilibrium effects are larger or smaller for the reaction in bulk water, where there are more solvent molecules but they move shorter distances.

Bulk equilibrium solvation effects have been calculated at several points along a reaction path for both the nucleophilic substitution reaction $Cl^- + CH_3Cl$ and the addition reaction of OH^- to H_2CO by Jorgensen and co-workers (*97–99*) in which Monte Carlo simulations are used to let the water equilibrate. Although not all degrees of freedom have been included yet, and the simulations are entirely classical, the approach appears quite promising for putting profiles for solution-phase free energy of activation on a quantitative footing. In addition, one obtains information about changes in the average number of hydrogen bonds to the solute and in the average energy per hydrogen bond as the system proceeds along the reaction path. There has also been some work in which analytic (nonsimulation) methods (*100*) are used to calculate the solvation contributions to $\Delta G^{GT,0}(T,s)$. Such approaches, if successful, can be used for exploratory studies on a wider number of systems.

Heterogeneous Catalysis

Reaction-path methods can also be applied to reactions at solid surfaces. Two examples are the surface diffusion of hydrogen atoms and dissociative chemisorption of hydrogen molecules.

The surface diffusion of an adatom may be considered as a prototype unimolecular reaction, for example,

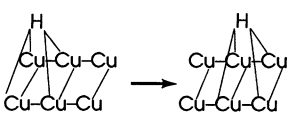

is a schematic, chemical way to depict the movement of a hydrogen atom from one fourfold bonding site on the (100) face of a copper surface to another one. The minimum energy path involves motion of the Cu atoms as well as the H, and it has been studied by embedded cluster calculations with an empirical PEF (*101, 102*). It is encouraging that reaction-path tunneling calculations agree with semiclassical simulations based on entirely different techniques (*103*) to within a factor of 1.6 even quite far into the quantum regime, where the semiclassical rates are more than three orders of magnitude larger than purely classical results (*101*). Reaction-path calculations have been performed with up to 87 degrees of freedom included in the kinetic energy (*102*). At 300 K the diffusion rates are converged with respect to the number of phonon modes included in the calculation when 18 phonon modes are included, but at 100 K the difference between tunneling along the MEP and tunneling calculated by the SCSAG approximation is still not converged with 84 phonon modes. This illustrates the important role of mode coupling in the quantal tunneling path.

More recently reaction-path methods have been extended to calculate chemisorption of H_2 on Ni (*104*), including dissociation at a step, and to model desorption of H_2 from Cu (*105*).

Conclusions

We have seen that very complex chemical processes can be described with a minimum of electronic structure information by concentrating attention on a tube of configuration space centered on a reaction path. Even when the dynamical path differs in a systematic way from the minimum-energy path, as in quantum mechanical tunneling processes, the dynamics can often be calculated conveniently and accurately in terms of the curvature of the minimum energy path and a power series expansion of the potential valley in its vicinity. In cases of very large reaction-path curvature, tunneling paths differing greatly from minimum-energy paths have been used to provide a description of quantum tunneling processes in terms of other local features of potential energy functions.

REFERENCES AND NOTES

1. According to the Born-Oppenheimer approximation, the potential energy for interatomic motion is the sum of the electronic energy (kinetic and potential) plus the internuclear coulomb repulsion energy. This sum as a function of the atomic coordinates is called the potential energy surface or potential energy function (PEF). In quantum mechanics the PEF determines the dynamics directly, but in classical mechanics one usually works with the interatomic forces, which are first derivatives of the PEF with respect to atomic positions, and the force field consists of these forces as functions of atomic positions.
2. F. London, *Z. Elektrochem.* **35**, 552 (1929); H. Eyring and J. Polanyi, *Naturwissenschaften* **18**, 914 (1930); *Z. Phys. Chem. Leipzig* **B12**, 279 (1931); S. Sato, *J. Chem. Phys.* **23**, 592 (1955).
3. C. A. Parr and D. G. Truhlar, *J. Phys. Chem.* **75**, 1844 (1971).
4. W. J. Hehre, L. Radom, P. v. R. Schleyer, J. A. Pople, *Ab Initio Molecular Orbital Theory* (Wiley, New York, 1986).
5. C. W. Bauschlicher, R. S. Langhoff, P. R. Taylor, *Adv. Chem. Phys.*, in press.
6. D. L. Bunker and M. D. Pattengill, *J. Chem. Phys.* **53**, 3041 (1970); L. M. Raff, *ibid.* **60**, 2220 (1974).
7. T. Joseph, R. Steckler, D. G. Truhlar, *ibid.* **87**, 7036 (1987).
8. J. N. Murrell, S. Carter, S. C. Farantos, P. Huxley, A. J. C. Varandas, *Molecular Potential Energy Functions* (Wiley, New York, 1984); D. G. Truhlar, R. Steckler, M. S. Gordon, *Chem. Rev.* **87**, 217 (1987); G. C. Schatz, *Rev. Mod. Phys.* **61**, 669 (1989).
9. S. Glasstone, K. J. Laidler, H. Eyring, *The Theory of Rate Processes* (McGraw-Hill, New York, 1941); D. G. Truhlar, W. L. Hase, J. T. Hynes, *J. Phys. Chem.* **87**, 2664 (1983); *ibid.*, p. 5223(E); M. M. Kreevoy and D. G. Truhlar, in *Investigation of Rates and Mechanisms of Reactions, Part 1*, C. Bernasconi, Ed. (Wiley, New York, ed. 4, 1986), pp. 13–95.
10. H. B. Schlegel, *Adv. Chem. Phys.* **67**, 249 (1987); H. B. Schlegel, in *New Theoretical Concepts for Understanding Organic Reactions*, J. Bertrán and I. G. Csizmadia, Eds. (Kluwer, Dordrecht, 1989), pp. 33–53.
11. E. B. Wilson, Jr., J. C. Decius, P. C. Cross, *Molecular Vibrations* (McGraw-Hill, New York, 1955), p. 14.
12. I. Shavitt, *Theoretical Chemistry Laboratory Report No. WIS-AEC-23* (University of Wisconsin, Madison, 1959); R. E. Weston, Jr., *J. Chem. Phys.* **31**, 892 (1959); I. Shavitt, *ibid.* **49**, 4048 (1968).
13. R. A. Marcus, *J. Chem. Phys.* **45**, 4493 (1966); *ibid.* **49**, 2610 (1968); *ibid.*, p. 2617.
14. D. G. Truhlar and A. Kuppermann, *J. Am. Chem. Soc.* **93**, 1840 (1971).
15. K. Fukui, in *The World of Quantum Chemistry*, R. Daudel and B. Pullman, Eds. (Reidel, Dordrecht, 1974), pp. 113–141.
16. H. F. Schaefer III, *Chem. Brit.* **11**, 227 (1975).
17. L. Hofacker, *Z. Naturforsch.* **18a**, 607 (1963); R. A. Marcus, *J. Chem. Phys.* **41**, 610 (1964); S. F. Fischer, G. L. Hofacker, R. Seiler, *ibid.* **51**, 3951 (1969).
18. R. A. Marcus, *J. Chem. Phys.* **45**, 4500 (1966).
19. W. H. Miller, N. C. Handy, J. E. Adams, *ibid.* **72**, 99 (1980); W. H. Miller, in *The Theory of Chemical Reaction Dynamics*, D. C. Clary, Ed. (Reidel, Dordrecht, 1986), pp. 27–45.
20. B. C. Garrett, D. G. Truhlar, R. S. Grev, A. W. Magnuson, *J. Phys. Chem.* **84**, 1730 (1980).
21. B. C. Garrett and D. G. Truhlar, *J. Chem. Phys.* **70**, 1593 (1979).
22. E. Wigner, *ibid.* **5**, 720 (1937); J. C. Keck, *Adv. Chem. Phys.* **13**, 85 (1967); S. C. Tucker and D. G. Truhlar, in *New Theoretical Concepts for Understanding Organic Reactions*, J. Bertrán and I. G. Csizmadia, Eds. (Kluwer, Dordrecht, 1989), pp. 291–346.
23. M. A. Eliason and J. O. Hirschfelder, *J. Chem. Phys.* **30**, 1426 (1959); R. A. Marcus, *ibid.* **45**, 2138 (1966); *ibid.* **46**, 959 (1967); D. G. Truhlar, *ibid.* **53**, 2041 (1970).
24. B. C. Garrett and D. G. Truhlar, *J. Phys. Chem.* **83**, 1052 (1979); *ibid.*, p. 1079.
25. A. Tweedale and K. J. Laidler, *J. Chem. Phys.* **53**, 2045 (1970).
26. B. C. Garrett and D. G. Truhlar, *J. Am. Chem. Soc.* **101**, 4534 (1979).
27. R. A. Marcus and M. E. Coltrin, *J. Chem. Phys.* **67**, 2609 (1977); B. C. Garrett and D. G. Truhlar, *Proc. Natl. Acad. Sci. U.S.A.* **76**, 4755 (1979); *J. Chem. Phys.* **77**, 5955 (1982).
28. R. T. Skodje, D. G. Truhlar, B. C. Garrett, *J. Phys. Chem.* **85**, 3019 (1981).
29. A. I. Shushin and M. Ya. Ovchinnikova, *Theor. Exp. Chem.* **11**, 374 (1975) [translation from *Teor. Eksperim. Khim.* **11**, 445 (1975)]; R. A. Marcus, in *Physicochemical Hydrodynamics*, D. B. Spalding, Ed. (Advance, Guernsey, United Kingdom, 1977), vol. 1, pp. 473–482; V. K. Babamov and R. A. Marcus, *J. Chem. Phys.* **74**, 1790 (1981); M. Ya. Ovchinnikova, *Chem. Phys.* **36**, 85 (1979).
30. B. C. Garrett, D. G. Truhlar, A. F. Wagner, T. H. Dunning, Jr., *J. Chem. Phys.*

78, 4400 (1983); D. K. Bondi, J. N. L. Connor, B. C. Garrett, D. G. Truhlar, *ibid.*, p. 5981.
31. D. G. Truhlar, A. D. Isaacson, B. C. Garrett, in *Theory of Chemical Reaction Dynamics*, M. Baer, Ed. (CRC Press, Boca Raton, FL, 1985), vol. 4, pp. 65–137.
32. R. K. Boyd, *Chem. Rev.* 77, 93 (1977); C. Lim and D. G. Truhlar, *J. Phys. Chem.* **90**, 2616 (1986).
33. A. D. Isaacson and D. G. Truhlar, *J. Chem. Phys.* 76, 1380 (1982).
34. B. C. Garrett and D. G. Truhlar, *ibid.* **81**, 309 (1984).
35. D. G. Truhlar and A. D. Isaacson, *ibid.* 77, 3516 (1982).
36. R. Steckler, D. G. Truhlar, B. C. Garrett, N. C. Blais, R. B. Walker, *ibid.* **81**, 5706 (1984); B. C. Garrett and D. G. Truhlar, *J. Phys. Chem.* **89**, 2204 (1985); *Int. J. Quantum Chem.* **29**, 1463 (1986); R. Steckler, D. G. Truhlar, B. C. Garrett, *J. Chem. Phys.* **84**, 6712 (1986); B. C. Garrett, D. G. Truhlar, J. M. Bowman, A. F. Wagner, *J. Phys. Chem.* **90**, 4305 (1986).
37. S. Koseki and M. S. Godon, *J. Phys. Chem.* **93**, 118 (1989).
38. M. S. Child, in *Theory of Chemical Reaction Dynamics*, M. Baer, Ed. (CRC Press, Boca Raton, FL, 1985), vol. 3, pp. 247–278.
39. B. C. Garrett and D. G. Truhlar, *J. Chem. Phys.* **79**, 4931 (1983).
40. B. C. Garrett, T. Joseph, T. N. Truong, D. G. Truhlar, *Chem. Phys.* **136**, 271 (1989).
41. B. Liu, *J. Chem. Phys.* **58**, 1925 (1973); P. Siegbahn and B. Liu, *ibid.* **68**, 2457 (1978); D. G. Truhlar and C. J. Horowitz, *ibid.*, p. 2466; *ibid.* **71**, 1514(E) (1979); M. R. A. Blomberg and B. Liu, *ibid.* **82**, 1050 (1985); A. J. C. Varandas, F. B. Brown, C. A. Mead, D. G. Truhlar, N. C. Blais, *ibid.* **86**, 6258 (1987).
42. R. Schinke and W. A. Lester, Jr., *ibid.* **70**, 4893 (1979); *ibid.* **72**, 3754 (1980).
43. N. Sathyamurthy and L. M. Raff, *ibid.* **63**, 464 (1975).
44. D. R. McLaughlin and D. L. Thompson, *ibid.* **59**, 4393 (1973).
45. S. P. Walch and T. H. Dunning, *ibid.* **72**, 1303 (1980); G. C. Schatz and H. Elgersma, *Chem. Phys. Lett.* **73**, 21 (1980).
46. R. J. Duchovic, W. L. Hase, H. B. Schlegel, *J. Phys. Chem.* **88**, 1339 (1984).
47. R. Viswanathan, D. L. Thompson, L. M. Raff, *J. Chem. Phys.* **80**, 4230 (1984).
48. C. S. Sloane and W. L. Hase, *Faraday Discuss. Chem. Soc.* **62**, 210 (1977).
49. M. Baer and I. Last, in *Potential Energy Surfaces and Dynamics Calculations*, D. G. Truhlar, Ed. (Plenum, New York, 1981), pp. 519–534; D. W. Schwenke *et al.*, *J. Chem. Phys.* **90**, 3110 (1989).
50. N. C. Blais and D. G. Truhlar, *J. Chem. Phys.* **61**, 4186 (1974); *ibid.* **65**, 3803(E) (1976); *ibid.* **83**, 5546 (1985).
51. F. B. Brown, R. Steckler, D. W. Schwenke, D. G. Truhlar, B. C. Garrett, *ibid.* **82**, 188 (1985).
52. R. K. Preston and J. C. Tully, *ibid.* **54**, 4297 (1971).
53. R. Viswanathan, D. L. Thompson, and L. M. Raff, *J. Phys. Chem.* **89**, 1428 (1985).
54. C. W. Eaker and C. A. Parr, *J. Chem. Phys.* **64**, 1322 (1976); P. A. Whitlock, J. T. Muckerman, P. M. Kroger, in *Potential Energy Surfaces and Dynamics Calculations*, D. G. Truhlar, Ed. (Plenum, New York, 1981), pp. 551–586.
55. D. G. Truhlar and R. E. Wyatt, *Adv. Chem. Phys.* **36**, 141 (1977).
56. A. Gonzalez-Lafont, T. N. Truong, D. G. Truhlar, unpublished calculations.
57. K. Ishida, K. Morokuma, A. Komornicki, *J. Chem. Phys.* 66, 2153 (1977); D. G. Truhlar, F. Brown, R. Steckler, A. D. Isaacson, in *The Theory of Chemical Reaction Dynamics*, D. C. Clary, Ed. (Reidel, Dordrecht, 1986), pp. 285–379; M. W. Schmidt, M. S. Gordon, M. Dupuis, *J. Am. Chem. Soc.* **107**, 2585 (1985).
58. T. H. Dunning, Jr., E. Kraka, R. A. Eades, *Faraday Discuss. Chem. Soc.* **84**, 427 (1987); T. H. Dunning, Jr., L. B. Harding, E. Kraka, in *Supercomputer Algorithms for Reactivity, Dynamics, and Kinetics of Small Molecules*, A. Laganà, Ed. (Kluwer, Dordrecht, 1989), pp. 57–71.
59. M. Page and J. W. McIver, Jr., *J. Chem. Phys.* **88**, 15 (1988). See also C. Doubleday, Jr., J. W. McIver, Jr., M. Page, *J. Phys. Chem.* **92**, 4367 (1988).
60. B. C. Garrett *et al.*, *J. Phys. Chem.* **92**, 1476 (1988).
61. J. Ischtwan and M. A. Collins, *J. Chem. Phys.* **89**, 2881 (1988).
62. K. K. Baldridge, M. S. Gordon, R. Steckler, D. G. Truhlar, *J. Phys. Chem.* **93**, 5107 (1989).
63. M. Page, paper E-14 presented at the Second International Conference on Chemical Kinetics, National Institute of Standards and Technology, Gaithersburg, MD, 24–27 July 1989.
64. C. Gonzalez and H. B. Schlegel, *J. Chem. Phys.* **90**, 2154 (1989).
65. V. Melissas, R. Steckler, B. C. Garrett, D. G. Truhlar, unpublished calculations.
66. B. C. Garrett, N. Abusalbi, D. J. Kouri, B. C. Garrett, D. G. Truhlar, *J. Chem. Phys.* **83**, 2252 (1985).
67. D. C. Clary, *ibid.*, p. 1685; B. C. Garrett, D. G. Truhlar, G. C. Schatz, *J. Am. Chem. Soc.* **108**, 2876 (1986); G. C. Lynch, D. G. Truhlar, B. C. Garrett, *J. Chem. Phys.* **90**, 3102 (1989).
68. K. Haug *et al.*, *J. Chem. Phys.* **87**, 1892 (1987); J. Z. H. Zhang *et al.*, *Faraday Discuss. Chem. Soc.* **84**, 371 (1987).
69. B. C. Garrett and D. G. Truhlar, *Int. J. Quantum Chem.* **31**, 17 (1987); G. C. Lynch *et al.*, *Z. Naturforsch.* **44a**, 427 (1989).
70. G. C. Schatz, B. Amaee, J. N. L. Connor, *Computer Phys. Commun.* **47**, 45 (1987).
71. M. M. Kreevoy, D. Ostović, D. G. Truhlar, B. C. Garrett, *J. Phys. Chem.* **90**, 3766 (1986).
72. J. Bicerano, H. F. Schaefer III, W. H. Miller, *J. Am. Chem. Soc.* **105**, 2550 (1983); T. Carrington and W. H. Miller, *J. Chem. Phys.* **84**, 4364 (1986); N. Shida, P. F. Barbara, J. E. Almlöf, *ibid.* **91**, 4061 (1989).
73. K. Haug *et al.*, *J. Phys. Chem.* **90**, 6757 (1986).
74. R. D. Levine, *Chem. Phys. Lett.* **10**, 510 (1971); G. L. Hofacker and R. D. Levine, *ibid.* **15**, 165 (1972); G. L. Hofacker and K. W. Michel, *Ber. Bunsenges. Phys. Chem.* **78**, 174 (1974); J. W. Duff and D. G. Truhlar, *J. Chem. Phys.* **62**, 2477 (1975); D. G. Truhlar and D. A. Dixon, in *Atom-Molecule Collision Theory*, R. B. Bernstein, Ed. (Plenum, New York, 1979), pp. 595–646; M. Sizun and S. Goursand, *Chem. Phys. Lett.* **79**, 269 (1981); R. T. Skodje, D. W. Schwenke, D. G. Truhlar, R. S. Grev, *J. Phys. Chem.* **88**, 628 (1984); R. T. Skodje and D. G. Truhlar, *J. Chem. Phys.* **80**, 3123 (1984).
75. B. Hartke and J. Manz, *J. Am. Chem. Soc.* **110**, 3063 (1988).
76. S. K. Gray, W. H. Miller, Y. Yamaguchi, H. F. Schaefer III, *J. Chem. Phys.* **73**, 2733 (1980); *J. Am. Chem. Soc.* **103**, 1900 (1981); A. Tachibana, I. Okazaki, M. Koizumi, K. Hori, T. Yomabe, *ibid.* **107**, 1190 (1985); S. M. Colwell and N. C. Handy, *J. Chem. Phys.* **82**, 128 (1985); S. M. Colwell, *Theor. Chim. Acta* **74**, 123 (1988).
77. A. D. Issacson *et al.*, *Computer Phys. Commun.* **47**, 91 (1987).
78. M. J. Rabinowitz, J. W. Sutherland, P. M. Patterson, R. B. Klemm, *J. Phys. Chem.*, in press.
79. J. A. Boatz and M. S. Gordon, *ibid.* **93**, 1819 (1989); *ibid.*, p. 5774.
80. H. Tachibana, K. Hori, Y. Asai, T. Yomabe, K. Fukui, *J. Mol. Struct. (Theochem.)* **123**, 267 (1965).
81. A. Tachibana, Y. Asai, M. Kohno, K. Hori, T. Yomabe, *J. Chem. Phys.* **83**, 6334 (1985).
82. G. Leroy, M. Sana, L. A. Burke, M. T. Nguyen, in *Quantum Theory of Chemical Reactions*, R. Daudel, A. Pullman, L. Salem, A. Veillard, Eds. (Reidel, Dordrecht, 1980), vol. 1, pp. 94–141; R. Daudel, *J. Mol. Struct. (Theochem.)* **103**, 269 (1983); K. Fukui, in *Applied Quantum Chemistry*, V. H. Smith, H. F. Schaefer, K. Morokuma, Eds. (Reidel, Dordrecht, 1986), pp. 1–25.
83. T. L. Windus, M. S. Gordon, L. P. Davis, L. W. Burggraf, unpublished results.
84. M. S. Gordon, L. P. Davis, L. W. Burggraf, R. Damrauer, *J. Am. Chem. Soc.* **108**, 7889 (1986).
85. K. K. Baldridge and M. S. Gordon, unpublished results.
86. J. Jensen and M. S. Gordon, unpublished results.
87. K. N. Houk and N. G. Rondan, *J. Am. Chem. Soc.* **106**, 4293 (1984); K. N. Houk, N. G. Rondan, J. Mareda, *Tetrahedron* **41**, 1555 (1985).
88. J. F. Blake, S. G. Wierschke, W. L. Jorgensen, *J. Am. Chem. Soc.* **111**, 1919 (1989).
89. W. L. Hase, *J. Chem. Phys.* **64**, 2442 (1976); *Acc. Chem. Res.* 16, 258 (1983).
90. S. N. Rai and D. G. Truhlar, *J. Chem. Phys.* **79**, 6046 (1983); X. Hu and W. L. Hase, *J. Phys. Chem.* **93**, 6029 (1989).
91. C. Doubleday, Jr., *et al.*, *J. Am. Chem. Soc.* **106**, 447 (1984).
92. C. Doubleday, J. McIver, M. Page, T. Zielinski, *ibid.* **107**, 5800 (1985).
93. K. Morokuma and S. Kato, in *Potential Energy Surfaces and Dynamics Calculations*, D. G. Truhlar, Ed. (Plenum, New York, 1981), pp. 243–264; K. Morokuma, S. Kato, K. Kitaura, S. Obara, K. Ohta, M. Hanamura, in *New Horizons of Quantum Chemistry*, P.-O. Löwdin and B. Pullman, Eds. (Reidel, Dordrecht, 1983), pp. 221–241; K. Morokuma, K. Yamashita, S. Yabushita, in *Supercomputer Algorithms for Reactivity, Dynamics, and Kinetics of Small Molecules*, A. Laganà, Ed. (Kluwer, Dordrecht, 1989), pp. 37–56.
94. S. C. Tucker and D. G. Truhlar, *J. Am. Chem. Soc.* **112**, 3347 (1990).
95. S. Baer, O. Stoutland, J. I. Brauman, *ibid.* **111**, 4097 (1989).
96. J. L. Kurz, *ibid.*, p. 8631, and references therein.
97. J. Chandrasekhar, S. F. Smith, W. L. Jorgensen, *ibid.* **106**, 3049 (1984); *ibid.* **107**, 154 (1985); J. Chandrasekhar and W. L. Jorgensen, *ibid.*, p. 2974.
98. J. D. Madura and W. L. Jorgensen, *ibid.* **108**, 2517 (1986); W. L. Jorgensen, *Adv. Chem. Phys.* **70**, 469 (1988); ———, J. F. Blake, J. D. Madura, S. D. Wierschke, *ACS Symp. Ser.* **353**, 200 (1987).
99. W. L. Jorgensen, J. K. Buckner, S. E. Huston, P. J. Rossky, *J. Am. Chem. Soc.* **109**, 1891 (1987).
100. S. E. Huston, P. J Rosky, D. A. Zichi, *ibid.* **111**, 5680 (1989); S. C. Tucker and D. G. Truhlar, *Chem. Phys. Lett.* **157**, 164 (1989).
101. J. G. Lauderdale and D. G. Truhlar, *Surf. Sci.* **164**, 558 (1985).
102. T. N. Truong and D. G. Truhlar, *J. Phys. Chem.* **91**, 6229 (1987).
103. S. M. Valone, A. F. Voter, J. D. Doll, *Surf. Sci.* **155**, 687 (1985).
104. T. N. Truong, G. C. Hancock, D. G. Truhlar, *ibid.* **214**, 523 (1989); T. N. Truong and D. G. Truhlar, *J. Phys. Chem.*, in press.
105. W. Brenig and H. Kasai, unpublished results.
106. We are very grateful to our many collaborators (see earlier references). This work was supported in part by the U.S. Department of Energy, Office of Basic Energy Sciences (VTST and tunneling calculations for reactions in the gas phase and solution) and the National Science Foundation, Air Force Office of Scientific Research, and Petroleum Research Fund (electronic structure calculations and dynamics at solid surfaces).

The optimum tunneling path depends on the curvature of the reaction path in mass-scaled coordinates.

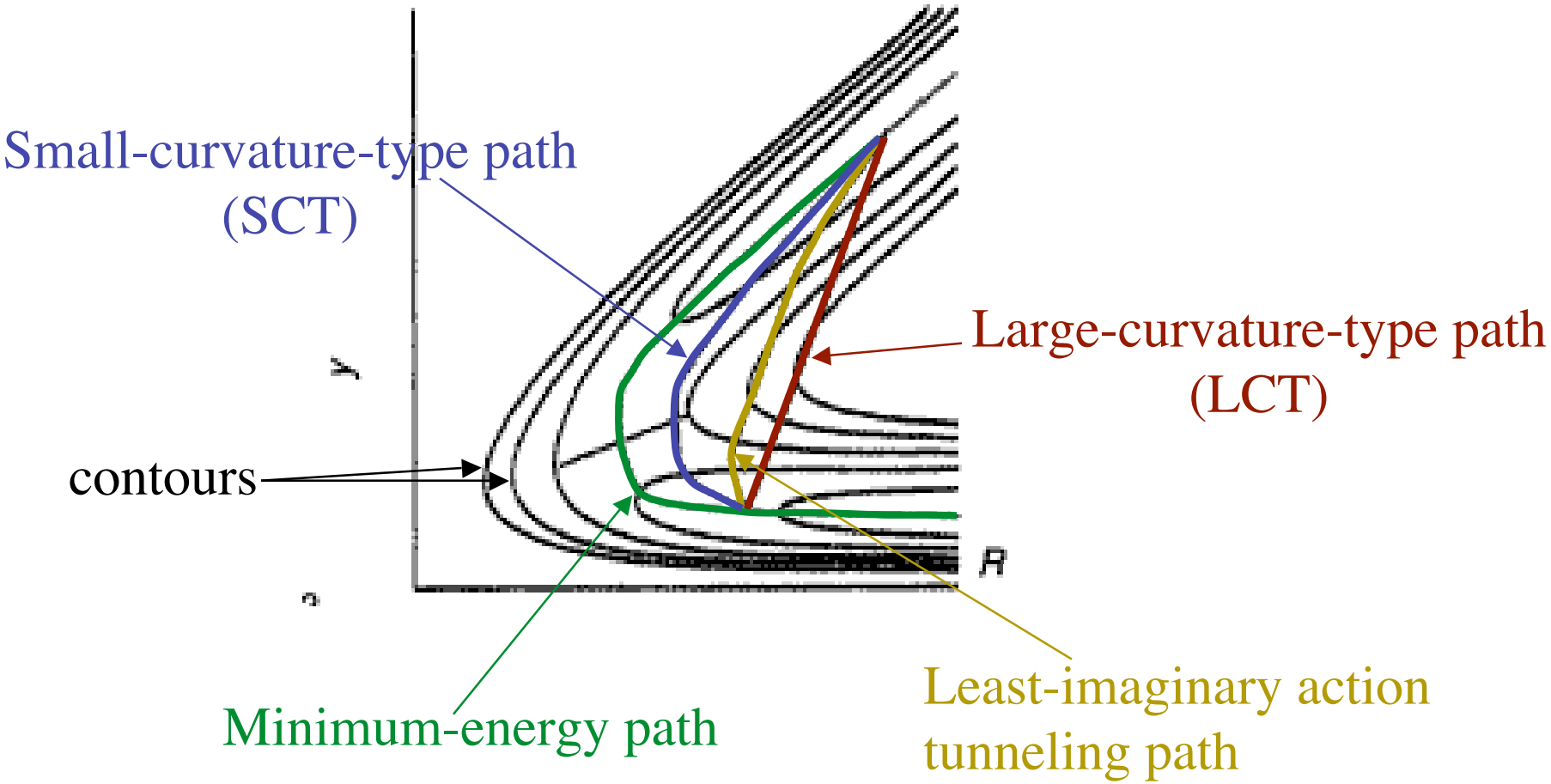

OMT = Optimized Multi-dimensional Tunneling $= \max \begin{cases} \text{SCT tun. prob.} \\ \text{LCT tun. prob.} \end{cases}$